

流れの非定常・カオス化と分岐構造

Bifurcation diagram and the onset of periodic and chaotic flows in a curved square duct

岡山大学工学部 柳瀬 真一郎 (Shinichiro Yanase)

Dept. of Mechanical Engg., Okayama University

岡山大学自然科学研究科 Rabindra Nath Mondal

Graduate School of Natural Sci. and Tech., Okayama University

同志社大学エネルギー変換研究センター 加賀 義人 (Yoshito Kaga)

*Research Center for Energy Conversion, Doshisha University***Abstract**

A numerical study is presented for the isothermal and non-isothermal flows in a curved square duct for the curvature, δ , in the range $0 < \delta \leq 0.5$ over a wide range of the Dean number. A temperature difference is applied between the vertical sidewalls for the Grashof number in the range $0 \leq Gr \leq 500$, where the outer wall is heated and the inner one is cooled. First, steady solutions are obtained by the Newton-Raphson iteration method. Linear stability of the steady solutions is then investigated. When there is no stable steady solution, time evolution calculations as well as their spectral analyses show that the steady flow turns into chaos through periodic or multi-periodic flows, if the Dean number is increased no matter what the curvature is, and the transition to periodic or the chaotic state is retarded consistently with the increase of curvature whether the flow is isothermal or non-isothermal. Convective heat transfer is found to be significantly enhanced by the secondary flow particularly when the Dean vortices emerge at the outer sidewall.

1. Introduction

Curved ducts are extensively used in many industrial applications, such as air conditioning systems, heat exchangers, cooling systems, and the blade to blade passage in modern gas turbines. Curved diffusing passages are also found in human arterial system. The flow through a curved duct, driven by a pressure gradient, has been studied considerably because of its practical importance in chemical, mechanical and biological engineering. Such a flow is called a Dean flow after the comprehensive study by Dean [1]. This flow has also attracted much attention because of its physically interesting features under the action of the centrifugal force caused by the curvature of the duct. A secondary flow is induced by unbalance between the centrifugal force and the pressure gradient in a cross section of the duct. There have been made lots of theoretical and experimental works concerning the Dean flow for various shapes of the cross section, here the review articles by Berger et al. [2], Nandakumar and Masliyah [3], Itoh [4] and Berger [5] may be referred.

One of the interesting features of the curved duct flow may be the existence of multiple solutions. This means that there are many steady solutions for the same flow condition. Dennis and Ng [6], Nandakumar and Masliyah [7] and later Yanase, Gotoh and Yamamoto [8] studied dual solutions of the flow through a curved duct. Yang and Keller [9] studied the bifurcation of the flow for small curvature and found multiple branches of solutions. Detailed bifurcation structure and the linear stability of solutions for fully developed flows in a curved square duct was determined by Winters [10]. He found that there are many symmetric and asymmetric steady solutions among which linearly stable ones are few. Daskopoulos and Lenhoff [11] extended the work by Winters [10] to a higher Dean number, where no new solution branches were detected but four limit points on the isolated two-cell branch were found as the Dean number increased. Some of these points lead to solutions with six to eight vortices. Finlay and Nandakumar [12] investigated a flow with large aspect ratio by use of the perturbation method. The existence of the multiple solutions of the flow through a curved duct of the large aspect ratio was first studied by Yanase and Nishiyama [13], and they obtained two kinds of solutions: the two-vortex solution and the four-vortex solution for the same aspect ratio. Later, flows through a curved duct of rectangular cross section were studied numerically to put emphasis on bifurcation of the solution by Yanase *et al.* [14].

Other important aspect of the curved duct flow is the enhancement of thermal exchange between two differentially heated vertical sidewalls. Because it is possible that the secondary flow conveys heat and then increases heat flux between two sidewalls. Most of the published researches in curved channels performed experimental investigations of flows under the isothermal conditions for the aspect ratio of 1 to 12 and curvature ratio of 0.2 to 0.025, while experimental studies on non-isothermal flows are limited because of the difficulties associated with the measurement of fluid temperature profile. Cheng and Akiyama [15] and Mori *et al.* [16] numerically predicted steady, fully developed laminar forced convection in channels with the uniform heat flux boundary conditions. Cheng and Akiyama [15] studied the flows through a duct with the aspect ratio ranging from 0.2 to 5, whereas Mori *et al.* [16] employed a square channel. In both investigations, temperature and velocity results showed clear evidence of secondary flows. Ru and Chang [17] considered combined free and forced convections for fully developed flows in uniformly heated curved tubes. Ligrani *et al.* [18] studied channels of aspect ratio 40 and showed that the formation of secondary vortices is more affected by external heating at the outer wall than on the inner wall of the passage. Chandratilleke and Nursubyakto [19] presented numerical calculations to describe the secondary flow characteristics and convective heat transfer in the flow through curved rectangular ducts of aspect ratio ranging from 1 to 8 that were heated on the outer wall, where they studied for small Dean numbers and compared the numerical results with their experimental data. Wang and Yang [20] numerically studied the fully developed bifurcation structure and stability of the forced convection in a curved square duct flow. Recently, Yanase

et al. [21, 22] studied numerical predictions of isothermal and non-isothermal flows through a curved rectangular duct at a constant curvature $\delta = 0.1$ over a wide range of the Dean number. They also studied the effect of secondary flows on convective heat transfer for differentially heated vertical sidewalls. Very recently Mondal *et al.* [23] performed numerical investigations to show the relationship between the unsteady solutions and the bifurcation diagram with the effects of curvature for the isothermal flow through a curved square duct.

In the present paper, a comprehensive numerical study is presented for both the isothermal and non-isothermal flows through a curved duct of square cross section over the wide range of the curvature and the Dean number. Studying the effects of curvature on the flow characteristics as well as the effects of secondary flow on the convective heat transfer are the important objectives of the present paper.

2. Fundamental equations

Consider an incompressible viscous fluid streaming through a curved duct of square cross section whose width and height are $2d$ and $2h$ respectively. The flow is driven by a constant pressure gradient G along the center-line of the duct, i.e., the main flow in the z -direction as shown in Fig. 1. It is assumed that the flow is uniform in the z -direction and that the outer sidewall is heated while the inner one is cooled. The temperature of the outer wall is $T_0 + \Delta T$ and that of the inner wall is $T_0 - \Delta T$ where $\Delta T > 0$, δ being the curvature of the duct. Velocity components in the x -, y - and z -directions are u , v and w respectively. All the variables are made non-dimensionalized.

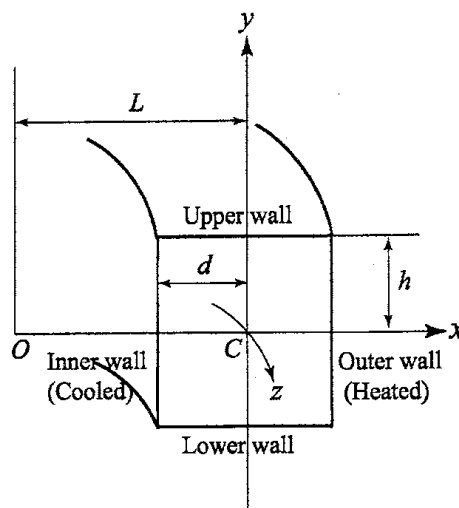


Figure 1: Coordinate system.

Since the flow field is uniform in the z -direction, the sectional stream function ψ

is introduced as

$$u = \frac{1}{1 + \delta x} \frac{\partial \psi}{\partial y}, \quad v = -\frac{1}{1 + \delta x} \frac{\partial \psi}{\partial x}. \quad (1)$$

The basic equations for w , ψ and T are derived from the Navier-Stokes equations and the energy equation under the *Boussinesq approximation* as,

$$(1 + \delta x) \frac{\partial w}{\partial t} + \frac{\partial(w, \psi)}{\partial(x, y)} - Dn + \frac{\delta^2 w}{1 + \delta x} = (1 + \delta x) \Delta_2 w - \frac{\delta}{(1 + \delta x)} \frac{\partial \psi}{\partial y} w + \delta \frac{\partial w}{\partial x}, \quad (2)$$

$$\begin{aligned} & \left(\Delta_2 - \frac{\delta}{1 + \delta x} \frac{\partial}{\partial x} \right) \frac{\partial \psi}{\partial t} = \\ & - \frac{1}{(1 + \delta x)} \frac{\partial(\Delta_2 \psi, \psi)}{\partial(x, y)} + \frac{\delta}{(1 + \delta x)^2} \left[\frac{\partial \psi}{\partial y} \left(2\Delta_2 \psi - \frac{3\delta}{1 + \delta x} \frac{\partial \psi}{\partial x} + \frac{\partial^2 \psi}{\partial x^2} \right) - \frac{\partial \psi}{\partial x} \frac{\partial^2 \psi}{\partial x \partial y} \right] \\ & + \frac{\delta}{(1 + \delta x)^2} \left[3\delta \frac{\partial^2 \psi}{\partial x^2} - \frac{3\delta^2}{1 + \delta x} \frac{\partial \psi}{\partial x} \right] - \frac{2\delta}{1 + \delta x} \frac{\partial}{\partial x} \Delta_2 \psi \\ & + w \frac{\partial w}{\partial y} + \Delta_2^2 \psi - Gr(1 + \delta x) \frac{\partial T}{\partial x}, \end{aligned} \quad (3)$$

$$\frac{\partial T}{\partial t} + \frac{1}{(1 + \delta x)} \frac{\partial(T, \psi)}{\partial(x, y)} = \frac{1}{Pr} \left(\Delta_2 T + \frac{\delta}{1 + \delta x} \frac{\partial T}{\partial x} \right) \quad (4)$$

where

$$\Delta_2 \equiv \frac{\partial^2}{\partial x^2} + \frac{\partial^2}{\partial y^2}, \quad \frac{\partial(f, g)}{\partial(x, y)} \equiv \frac{\partial f}{\partial x} \frac{\partial g}{\partial y} - \frac{\partial f}{\partial y} \frac{\partial g}{\partial x}. \quad (5)$$

In the above formulations, Dn is the Dean number, Gr the Grashof number and Pr the Prandtl number which are defined as $Dn = \frac{Gd^3}{\mu\nu} \sqrt{\frac{2d}{L}}$, $Gr = \frac{\gamma g \Delta T d^3}{\nu^2}$ and $Pr = \frac{\nu}{\kappa}$ respectively.

The rigid boundary conditions for w and ψ are used as

$$\left. \begin{aligned} w(\pm 1, y) = w(x, \pm 1) = \psi(\pm 1, y) = \psi(x, \pm 1) \\ = \frac{\partial \psi}{\partial x}(\pm 1, y) = \frac{\partial \psi}{\partial y}(x, \pm 1) = 0, \end{aligned} \right\} \quad (6)$$

and the temperature T is assumed to be constant on the walls as

$$T(1, y) = 1, \quad T(-1, y) = -1, \quad T(x, \pm 1) = x. \quad (7)$$

3. Numerical Calculations

In order to solve Eqs. (2) to (4) numerically, the spectral method is used in which variables are expanded in the series of functions consisting of the Chebyshev polynomials. That is, $\Phi_n(x)$ and $\Psi_n(x)$ are expressed as

$$\Phi_n(x) = (1 - x^2) C_n(x), \quad \Psi_n(x) = (1 - x^2)^2 C_n(x) \quad (8)$$

where $C_n(x) = \cos(n \cos^{-1}(x))$ is the n -th order Chebyshev polynomial. $w(x, y, t)$, $\psi(x, y, t)$ and $T(x, y, t)$ are expanded in terms of the expansion functions $\Phi_n(x)$ and

$\Psi_n(x)$ as

$$\left. \begin{aligned} w(x, y, t) &= \sum_{m=0}^M \sum_{n=0}^N w_{mn}(t) \Phi_m(x) \Phi_n(y), \\ \Psi(x, y, t) &= \sum_{m=0}^M \sum_{n=0}^N \psi_{mn}(t) \Psi_m(x) \Psi_n(y), \\ T(x, y, t) &= \sum_{m=0}^M \sum_{n=0}^N T_{mn}(t) \Phi_m(x) \Phi_n(y) + x, \end{aligned} \right\} \quad (9)$$

where M and N are the truncation numbers in the x - and y -directions respectively. It is assumed that the equations hold at the $(M+1)(N+1)$ collocation points (x_i, y_j) which are

$$x_i = \cos \left[\pi \left(1 - \frac{i}{M+2} \right) \right], \quad y_j = \cos \left[\pi \left(1 - \frac{j}{N+2} \right) \right] \quad (10)$$

where $i = 1, \dots, M+1$ and $j = 1, \dots, N+1$. In the present numerical calculations, $M = 20$ and $N = 40$ have been used for sufficient accuracy of the solutions.

First, steady solutions are obtained by the Newton-Raphson iteration method and then linear stability of the steady solutions is investigated against only two-dimensional (z -independent) perturbations. Finally, in order to calculate unsteady solutions, the Crank-Nicolson and Adams-Bashforth methods together with the function expansion (9) and the collocation methods are applied to Eqs. (2) to (4).

In this paper, numerical calculations are carried out for the curvature in the range $0 < \delta \leq 0.5$ over a wide range of the Dean number $0 \leq Dn \leq 8000$ for the isothermal flow ($Gr = 0$) and in $0 \leq Dn \leq 6000$ for the non-isothermal flow ($0 < Gr \leq 500$).

4. Resistance coefficient and the Nusselt number

In this study, the resistance coefficient λ is used as the representative quantity of the flow state. It is also called the *hydraulic resistance coefficient*, and is generally used in fluids engineering, defined as

$$\frac{P_1^* - P_2^*}{\Delta z^*} = \frac{\lambda}{4d} \rho \langle w^* \rangle^2 \quad (11)$$

where quantities with an asterisk denote dimensional ones, $\langle \rangle$ stands for the mean over the cross section of the duct and ρ is the density. The mean axial velocity $\langle w^* \rangle$ is calculated by

$$\langle w^* \rangle = \frac{\nu}{4\sqrt{2}\delta d} \int_{-1}^1 dx \int_{-1}^1 w(x, y, t) dy. \quad (12)$$

Since $(P_1^* - P_2^*)/\Delta z^* = G$, λ is related to the mean nondimensional axial velocity $\langle w \rangle$ as

$$\lambda = \frac{4\sqrt{2}\delta Dn}{\langle w \rangle^2}, \quad (13)$$

where $\langle w \rangle = \sqrt{2\delta}d\langle w^* \rangle/\nu$. In the present paper, λ is used to denote the steady solution branches and to pursue the time evolution of the unsteady solutions.

The Nusselt number, Nu , which is used as an index of the heat transfer from the walls to the fluid, is defined as

$$Nu_c = \frac{1}{2} \int_{-1}^1 \left[\frac{\partial T}{\partial x} \right]_{x=-1} dy, \quad Nu_h = \frac{1}{2} \int_{-1}^1 \left[\frac{\partial T}{\partial x} \right]_{x=1} dy \quad (14)$$

for steady solutions. For unsteady solutions, on the other hand, it is defined as

$$Nu_{\tau_c} = \frac{1}{2} \int_{-1}^1 \left\langle \left\langle \frac{\partial T}{\partial x} \right|_{x=-1} \right\rangle \right\rangle dy, \quad Nu_{\tau_h} = \frac{1}{2} \int_{-1}^1 \left\langle \left\langle \frac{\partial T}{\partial x} \right|_{x=1} \right\rangle \right\rangle dy, \quad (15)$$

where $\langle \rangle$ denotes an average over a time interval τ . When the field is periodic, τ is taken as one period, and if it is chaotic τ is chosen as an appropriate time interval.

5. Results and Discussion

5.1 Isothermal flow ($Gr = 0$)

5.1.1 Steady solutions and linear stability analysis

With the present numerical calculations, three branches of steady solutions are obtained for the smaller curvature ($\delta \leq 0.27$), for larger curvature ($\delta \geq 0.28$), on the other hand, we obtain two branches of steady solutions over a wide range of the Dean number $0 < Dn \leq 8000$. A bifurcation diagram, for example, is shown in Fig. 2 for $\delta = 0.1$ and $100 \leq Dn \leq 2000$ using λ , the representative quantity for the bifurcation analysis of the solutions. The three steady solution branches for $\delta \leq 0.27$ are named as the *first steady solution branch* (first branch, thick solid line), the *second steady solution branch* (second branch, dashed line) and the *third steady solution branch* (third branch, thin solid line) respectively. The solution branches are obtained by the path continuation technique with various initial guess and are distinguished by the nature and number of secondary flow vortices appearing in the cross section of the duct (for details, see Yanase *et al.*, [21]). It should be noted here that the bifurcation diagram for other values of δ is very similar to that for $\delta = 0.1$ if $\delta \leq 0.27$.

The first steady solution branch, obtained for $\delta \leq 0.27$, is a two- and four-vortex solutions. This is the only branch which exists throughout the whole range of the Dean number in the present study. The second steady solution branch is separated from the first branch by a subcritical pitchfork bifurcation at point p and extends up to point q on the third branch where it terminates and thus it makes a closed loop. An enlargement about point p and q are shown in Figs. 3(a) and 3(b) respectively where the ordinate $\iint \psi dx dy$ denotes the degree of asymmetry with respect to $y = 0$. The secondary flow patterns on the second branch show that it contains only asymmetric two-vortex solutions which are mirror symmetric with each other with respect to the plane $y = 0$. The third steady solution branch, which is very entangled

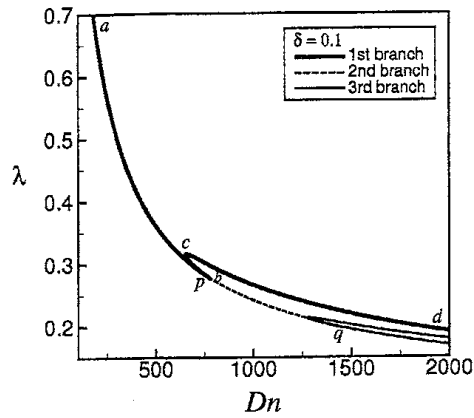


Figure 2: Steady solution branches for $Gr = 0$ and $100 \leq Dn \leq 2000$ at $\delta = 0.1$.

at larger Dean numbers, is composed of symmetric two- and multi-vortex solutions. The second branch, which is bifurcated from the first branch, terminates at point q on this branch. In this regard, it should be remarked that Winters [10] obtained the second branch to be nonterminating at any bifurcation point on any other branch. In the present study, however, it is found that the bifurcated branch terminates at the bifurcation point q on the third branch. Thus it is found that there exists a bifurcating relationship among the three branches of steady solutions obtained for $\delta \leq 0.27$.

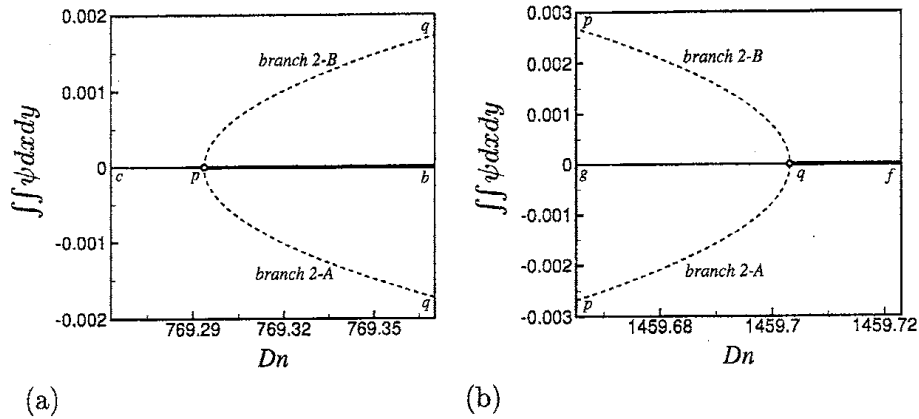


Figure 3: Second steady solution branch with enlargements at p and q , (a) subcritical pitchfork bifurcation, (b) super critical pitchfork bifurcation.

Linear stability of the steady solutions is then investigated. It is found that the first and third branches are linearly stable in two distinct ranges of the Dean number while the second branch is linearly unstable. Note that in the paper by Winters [10], the solution branch S_5 , which corresponds to the lower branch of the present third branch, consists of only two-vortex solution and that it is always stable. In the present study, however, it is found that the solution branch S_5 contains two- and

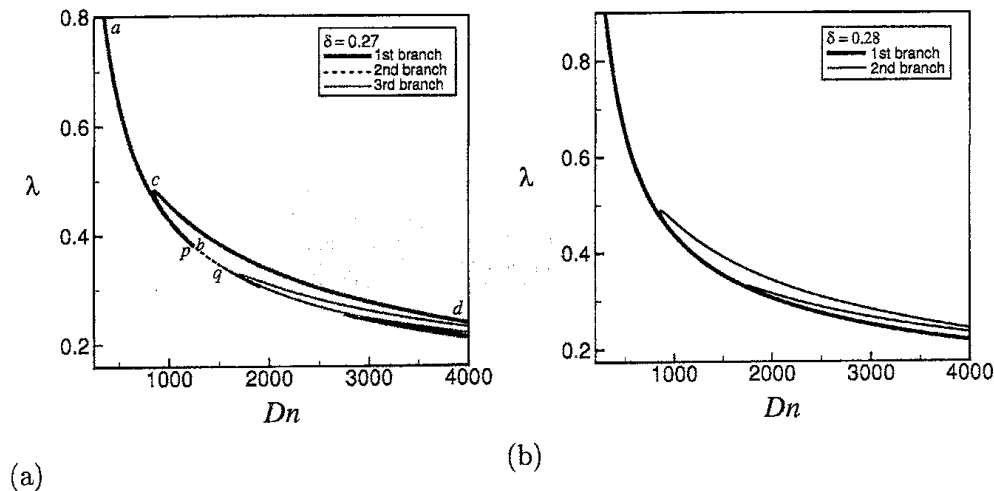


Figure 4: Steady solution branches for $Gr = 500$. (a) For $\delta = 0.27$ and $200 \leq Dn \leq 4000$. (b) For $\delta = 0.28$ and $200 \leq Dn \leq 4000$.

multi-vortex solutions, if the Dean number is increased, which is not always stable. The reason may be that Winters's calculation covered a comparatively small region of the Dean number.

In this study, it is found that if $\delta \geq 0.28$, the bifurcation diagram topologically changes from that obtained for $\delta \leq 0.27$. For $0.28 \leq \delta \leq 0.5$, we obtain two branches of steady solutions, where the branch consisting of the asymmetric solutions for $\delta \leq 0.27$ disappears. It can be inferred that the first and third branches, obtained for smaller curvature ($\delta \leq 0.27$), are reconnected to make the first and second branches for larger curvature ($\delta \geq 0.28$). The bifurcation diagrams for $\delta = 0.27$ and $\delta = 0.28$, for example, are shown in Figs. 4(a) and 4(b) respectively. The two steady solution branches for $\delta = 0.28$ are named as the *first steady solution branch* (first branch, thick solid line) and the *second steady solution branch* (second branch, thin solid line) respectively. It is found that the two solution branches are independent and there exists no bifurcating relationship between them in the parameter range investigated in this paper. The first steady solution branch for $0.28 \leq \delta \leq 0.5$ is a symmetric two-vortex solution while the second branch is of symmetric four-vortex solution. Linear stability analysis shows that only a limited portion of the first branch is linearly stable while the second branch is linearly unstable everywhere on it.

5.1.2 Time evolution and spectral analysis

In order to study the nonlinear behavior of the unsteady solutions, time evolution calculations as well as their spectral analysis are performed. Some of the results for $\delta = 0.1$ are discussed here, in brief, and the total unsteady solutions are presented in Fig. 7.

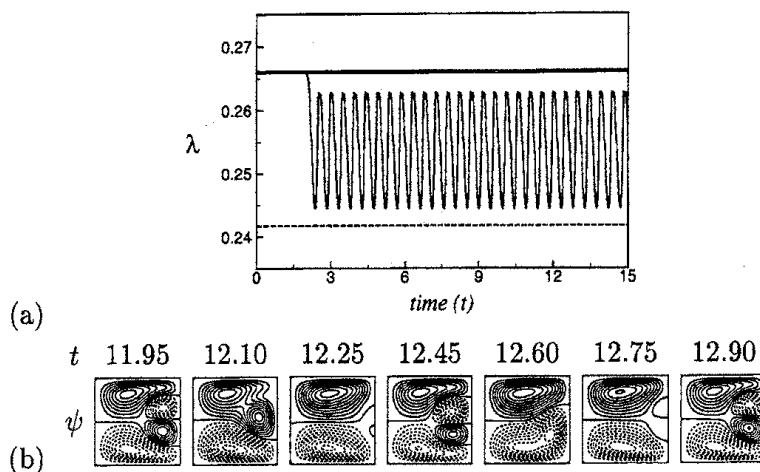


Figure 5: Results for $Dn = 1000$ and $Gr = 0$ at $\delta = 0.1$. (a) Time evolution of λ and the values of λ for the steady solutions for $0 \leq t \leq 15$, (b) contours of secondary flow for one period of oscillation at $11.95 \leq t \leq 12.90$.

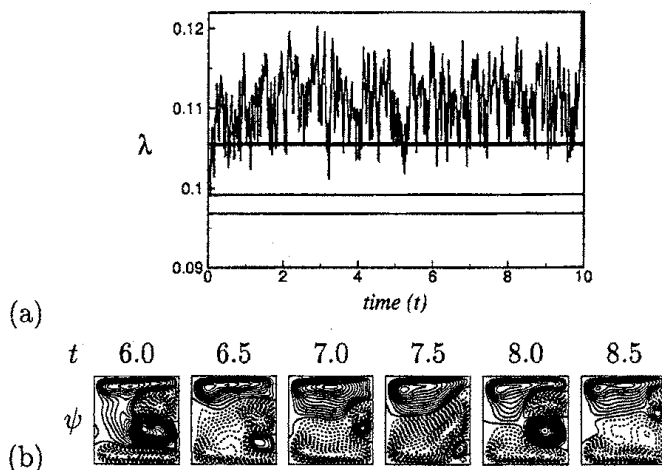


Figure 6: Results for $Dn = 7500$ and $Gr = 0$ at $\delta = 0.1$. (a) Time evolution of λ and the values of λ for the steady solutions for $0 \leq t \leq 10$, (b) contours of secondary flow for $6.0 \leq t \leq 8.5$.

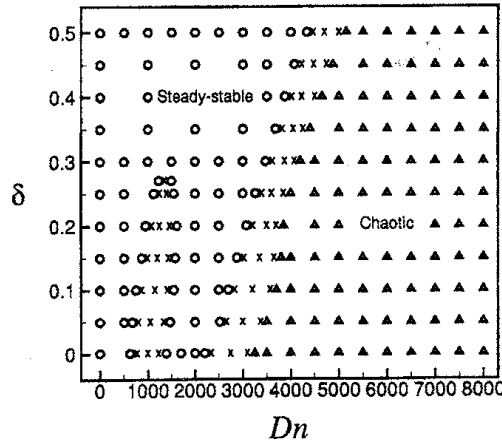


Figure 7: Time-dependent solutions in the Dean number vs. curvature ($Dn - \delta$) plane for $0 \leq Dn \leq 8000$ and $0 < \delta \leq 0.5$ for $Gr = 0$ (\circ : steady stable solution, \times : periodic solution and \triangle : chaotic solution).

Time evolutions of λ for $Dn \leq 782$ at $\delta = 0.1$ show that the flow is stable while those for $783 \leq Dn \leq 1459$ show that the unsteady flow oscillates periodically. Time evolution of λ for $Dn = 1000$, for example, is shown in Fig. 5(a) and the corresponding secondary flow in Fig. 5(b) where it is seen that the flow oscillates between the asymmetric two- and nearly symmetric four-vortex solutions, while the value of λ repeats the same oscillation twice in one period. Then time evolutions of λ for $1460 \leq Dn \leq 2770$ at $\delta = 0.1$ show that the flow becomes stable once again but those for $2771 \leq Dn \leq 3600$ show that the flow is periodic first and then multi-periodic, if the Dean number is increased. The chaotic solution is observed for $3700 \leq Dn \leq 8000$. It is found that the transition from periodic to chaotic state occurs between $Dn = 3600$ and $Dn = 3700$. A chaotic oscillation, for example, is shown in Fig. 6(a) and the secondary flow patterns in Fig. 6(b). The chaotic solutions for $Dn < 7500$ are considered to be the *weak chaos*, while those for $Dn \geq 7500$ the *strong chaos*, since the chaotic solutions for $Dn < 7500$ are still trapped among the steady solution branches but those for $Dn \geq 7500$ tend to get away from them. The power spectra of the time change of λ are performed to investigate the transition from a periodic solution to chaotic one and also to differ the strong chaos from that of the weak one. In this study, the time evolution calculations for other values of δ show that the time-dependent behavior is similar to that for $\delta = 0.1$. The distribution of the steady, periodic and chaotic solutions, obtained by the time evolution calculations, is presented in Fig. 7 in the Dean number versus curvature ($Dn - \delta$) plane, where the circle indicates stable steady solutions, the cross periodic solutions and the triangle chaotic solutions. As seen in Fig. 7, the steady flows turn to chaotic flows through periodic flows if the Dean number is increased no matter what the curvature is, though for smaller curvature ($\delta \leq 0.27$) a periodic

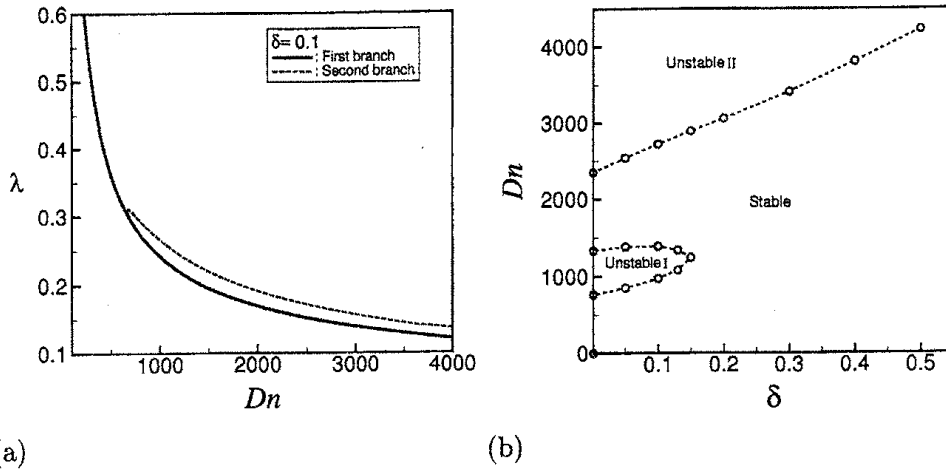


Figure 8: (a) Steady solution branches for $Gr = 500$ and $100 \leq Dn \leq 4000$ at $\delta = 0.1$. (b) Stability criterion in the Dean number vs. curvature ($Dn - \delta$) plane for $Gr = 500$.

solution returns to a steady solution once before turning to chaos. If the curvature is increased, the region of stable steady solution increases and consequently the occurrence of the periodic state and hence the chaotic state is delayed.

5.2 Non-isothermal flow ($0 < Gr \leq 500$)

5.2.1 Steady solutions and linear stability analysis

For the non-isothermal flow in the range of the Grashof number, Gr , $0 < Gr \leq 500$, we obtain two branches of steady solutions for the curvature, δ , in the range $0 < \delta \leq 0.5$ over a wide range of the Dean number $100 \leq Dn \leq 6000$. A bifurcation diagram, for example, is shown in Fig. 8(a) for $Gr = 500$ and $100 \leq Dn \leq 4000$ at $\delta = 0.1$ using λ , the representative quantity of the solutions. The two steady solution branches are named as the *first steady solution branch* (first branch, solid line) and the *second steady solution branch* (second branch, dashed line) respectively. The first branch varies monotonically as Dn increases, while the second branch consists of the upper and lower branches that are connected at a turning point. The first branch is an asymmetric two-vortex solution while the second branch is composed of asymmetric two- and four-vortex solutions. Heating the outer wall causes deformation of the secondary flow and yields asymmetry of the solution. Note that for other values of the curvature, the bifurcation diagram is topologically unchanged from Fig. 8(a). In this respect, it is interesting to note that for the isothermal flow, we observe a topological change of the bifurcation diagram when the curvature is increased from $\delta = 0.27$ to $\delta = 0.28$. For smaller curvature ($\delta \leq 0.27$), the bifurcation diagram remains topologically unchanged having three branches of steady solutions, for larger curvature ($\delta \geq 0.28$), on the other hand, we obtain other type of bifurcation diagram with two branches of solutions. For the case of non-

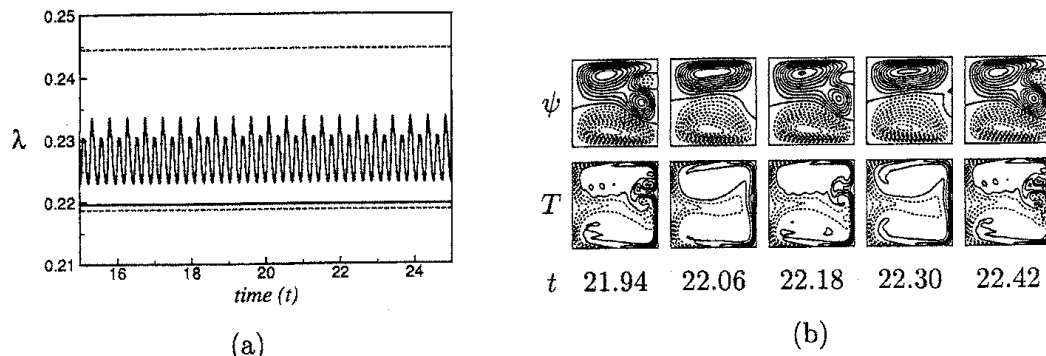


Figure 9: Results for $Dn = 1200$ and $Gr = 500$ at $\delta = 0.1$. (a) Time evolution of λ and the values of λ for the steady solutions for $15 \leq t \leq 25$, (b) contours of secondary flow (top) and temperature profile (bottom) for one period of oscillation at $21.94 \leq t \leq 22.42$.

isothermal flow, the bifurcation diagram at any δ , whether it is small or large, is similar to that for $\delta \geq 0.28$ of isothermal flow.

Linear stability of the steady solutions is then studied for various δ . It is found that only the first branch is linearly stable while the other branch is linearly unstable. The first branch is linearly stable in two different intervals of the Dean number for small curvature, for large curvature, on the other hand, the steady solution is stable in a single but wide interval of the Dean number. An example of the stability characteristics is illustrated in Fig. 8(b) for $0 < \delta \leq 0.5$ and $0 \leq Dn \leq 4500$ for $Gr = 500$. In this figure, the regions of stable and unstable solutions are separated by broken lines where the circles denote the stable solutions on the boundary line calculated in this study. As seen in Fig. 8(b), there exist two unstable regions. One unstable region, say region I, exists for smaller Dean numbers and suddenly vanishes as the Dean number increases. This region becomes narrower as δ increases and terminates at $\delta \approx 0.15$. The other unstable region, say region II, on the other hand, exists for larger Dean numbers and is not stabilized any more as the Dean number or the curvature increases. It is observed that the stability region in terms of the Dean number increases with the increase of curvature as seen in Fig. 8(b). Almost similar characteristics of the stability phenomena is observed for other Grashof numbers as well.

5.2.2 Time evolution and spectral analysis

Time evolution calculations as well as their spectral analysis are then performed for the non-isothermal flow at various Dn , δ and Gr . The time evolution results are not discussed here due to brevity, only two of them are discussed in short. Figure 9(a) shows a periodic solution for $Dn = 1200$ and $Gr = 500$ at $\delta = 0.1$ where the straight lines indicate the positions of the steady solutions. Contours of secondary flow for $Dn = 1200$ are shown in Fig 9(b) which shows that the periodic flow is a two-

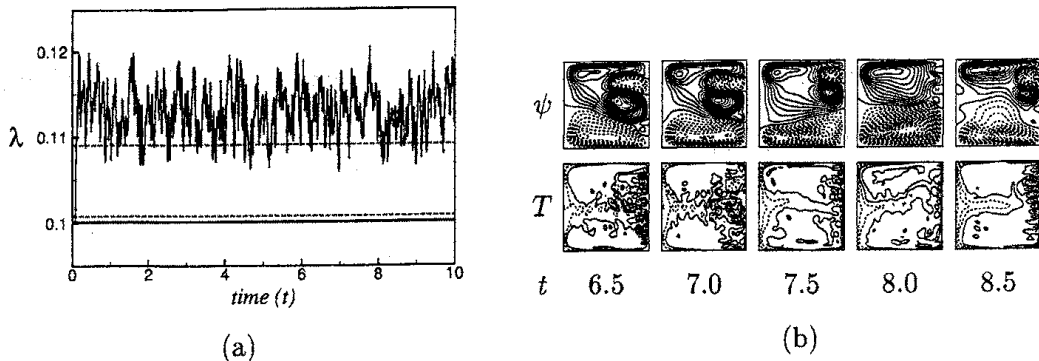


Figure 10: Results for $Dn = 6000$ and $Gr = 500$ at $\delta = 0.1$. (a) Time evolution of λ and the values of λ for the steady solutions for $0 \leq t \leq 10$, (b) contours of secondary flow (top) and temperature profile (bottom) for $6.5 \leq t \leq 8.5$.

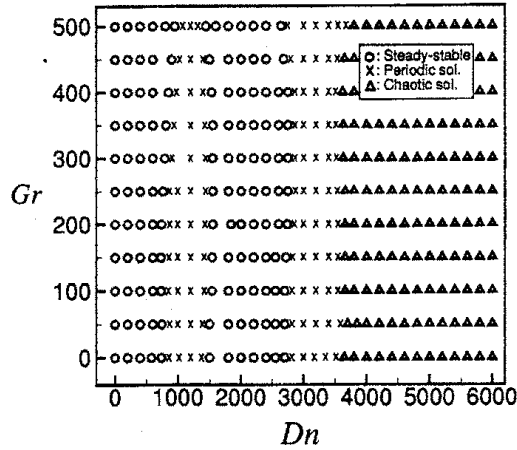


Figure 11: Time-dependent solutions in the Dean number vs. Grashof number ($Dn - Gr$) plane for $0 \leq Dn \leq 6000$ and $0 \leq Gr \leq 500$ for $\delta = 0.1$.

and four-vortex solutions. Figure 10(a) shows the chaotic oscillation for $Dn = 6000$ and $Gr = 500$ at $\delta = 0.1$. Corresponding secondary flow patterns are shown in Fig 10(b) which shows that the flow is a four-vortex solution. The total unsteady solutions, obtained by the time evolution calculations, are shown in Fig. 11 in the Dean number versus Grashof number plane for $0 \leq Dn \leq 6000$ and $0 \leq Gr \leq 500$ at $\delta = 0.1$. In this picture, the circles indicate stable steady solutions, the cross periodic solutions and the triangles chaotic solutions. For a specific Grashof number $Gr = 500$, the time-dependent solutions are also obtained varying curvature and we observe no qualitative change of the unsteady solutions as were observed in Fig. 7 for isothermal flow. The time evolution calculations for other values of Gr show that the time-dependent behavior is nearly similar to that for $Gr = 500$.

5.2.3 Nusselt number

The Nusselt number, Nu , defined in Eq. (14), can be used as an index of the horizontal heat transfer from the walls to the fluid. If the flow field is not steady, time-average of the Nusselt number, Nu_τ , is used which is defined in Eq. (15). To study the convective heat transfer for differentially heated vertical sidewalls, variation of the Nusselt number with the Dean number for the first steady solution branch at $\delta = 0.1$ is shown in Fig. 12, where a thick solid line denotes Nu_c on the inner (cooled) sidewall and a thin solid line Nu_h on the outer (heated) sidewall. In order to study the phenomena for the convective heat transfer from the walls to the fluid, temperature gradients on the inner and outer sidewalls are calculated which are shown in Figs. 13(a) and 13(b) respectively.

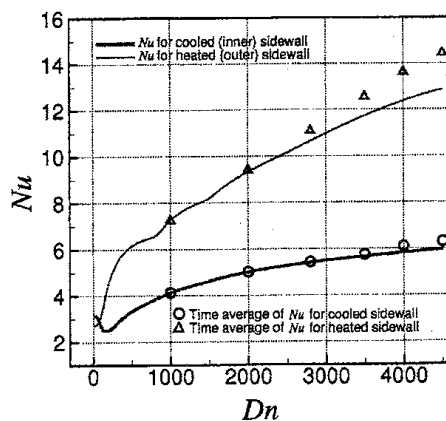


Figure 12: Variation of the Nusselt number with the Dean number for the first steady solution branch for $Gr = 500$ at $\delta = 0.1$.

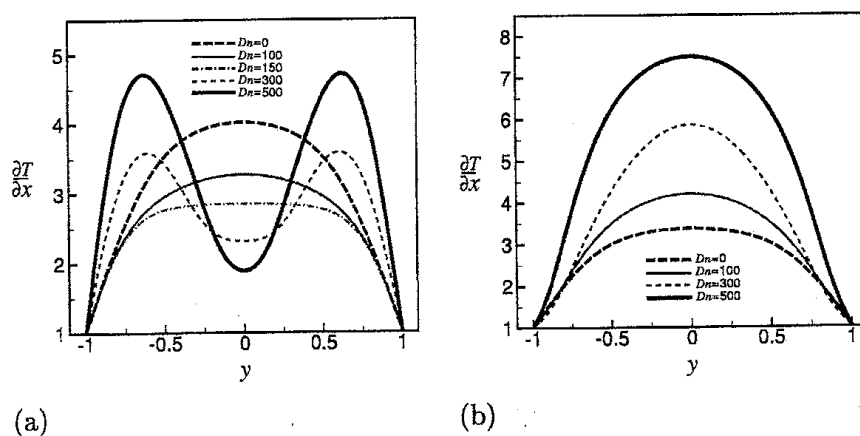


Figure 13 Temperature gradient for $Gr = 500$ at $\delta = 0.1$. (a) At the cooled sidewall, (b) at the heated sidewall.

Time-average of the Nusselt number, obtained by the time evolution computation of the Nusselt number for the inner and outer sidewalls, is calculated at several values of the Dean number for both the periodic and chaotic solutions and plotted with the steady values of the Nusselt number in Fig. 12. As seen in Fig. 12, time-averaged values of the Nusselt number are larger than the steady values of the Nusselt number for both the inner and outer sidewalls, which suggest that occurrence of the periodic or chaotic flow enhances heat transfer in the flow. It should be remarked that the tendency of increasing the Nusselt number is larger on the outer sidewall than that on the inner sidewall for larger Dean numbers, which can be explained by the fact that many subsidiary secondary vortices are generated near the outer sidewall [19]. To compare the convective heat transfer of a curved duct with that of a straight channel, an additional calculation of the Nusselt number for a straight channel is conducted and it is found that convective heat transfer is significantly enhanced by the curved duct than that in a straight channel, and that heat is transferred in a great deal as the secondary flow becomes stronger.

参考文献

- [1] W. R. Dean, 1927, Note on the motion of fluid in a curved pipe, *Philos. Mag.*, **5**, pp. 208-223.
- [2] S. A. Berger, L. Talbot and L. S. Yao, 1983, Flow in curved pipes, *Annu. Rev. Fluid. Mech.*, **15**, pp. 461-512.
- [3] K. Nandakumar and J. H. Masliyah, 1986, Swirling flow and heat transfer in coiled and twisted pipes, *Adv. Transp. Process.* **4**, pp. 49-112.
- [4] H. Ito, 1987, Flow in curved pipes, *JSME Int. J.*, **30**, pp. 543-552.
- [5] S. A. Berger 1991, Flow and heat transfer in curved pipes and tubes, *AIAA*, 91-0030, pp. 1-19.
- [6] S. C. R. Dennis and M. Ng, 1982, Dual solutions for steady laminar flow through a curved tube, *Quart. J. Mech. Appl. Math.*, **35**, pp. 305-324.
- [7] K. Nandakumar and J. H. Masliyah, 1982, Bifurcation in steady laminar flow through curved tubes, *J. Fluid Mech.*, **119**, pp. 475-490.
- [8] S. Yanase, N. Goto and K. Yamamoto, 1989, Dual solutions of the flow through a curved tube, *Fluid Dyn. Res.*, **5**, pp. 191-201.
- [9] Z. Yang and H. B. Keller, 1986, Multiple laminar flows through curved pipes, *Applied Numerical Mathematics*, **2**, pp. 257-271.
- [10] K. H. Winters, 1987, A bifurcation study of laminar flow in a curved tube of rectangular cross section, *J. Fluid Mech.*, **180**, pp. 343-369.

- [11] P. Daskopoulos and A. M. Lenhoff, 1990, Flow in curved ducts: Part 2, rotating ducts, *J. Fluid Mech.*, **217**, pp. 575-593.
- [12] W. H. Finlay K. and Nandakumar, 1990, Onset of two-dimensional cellular flow in finite curved channels of large aspect ratio, *Phys. Fluids A*, **2**, pp. 1163-1174.
- [13] S. Yanase and K. Nishiyama, 1988, On the bifurcation of laminar flows through a curved rectangular tube, *J. Phys. Soc. Jpn.*, **57**, pp. 3790-3795.
- [14] S. Yanase, Y. Kaga and R. Daikai, 2002, Laminar flows through a curved rectangular duct over a wide range of the aspect ratio, *Fluid Dyn. Res.*, **31**, pp. 151-183.
- [15] K. C. Cheng and M. Akiyama, 1970, Laminar forced convection heat transfer in curved rectangular channels, *Int. J. Heat Mass Transfer*, **13**, pp. 471-490.
- [16] Y. Mori, Y. Uchida and T. Ukon, 1971, Forced convective heat transfer in curved channel with a square cross section, *Int. J. Heat Mass Transfer*, **14**, pp. 1787-1805.
- [17] Y. Ru and S. F. Chang, 1994, Combined free and forced convection for developed flow in curved pipes with finite curvature ratio, *Int. J. Heat Fluid Flow*, **15** (6), pp. 470-476.
- [18] P. M. Ligrani, S. Choi, A. R. Scallert and P. Skogerboe, 1996, Effects of Dean vortex pairs on surface heat transfer in curved channel flow, *Int. J. Heat Mass Transfer*, **39**, pp. 27-37.
- [19] T. T. Chandratilleke and Nursubyakto, 2003, Numerical prediction of secondary flow and convective heat transfer in externally heated curved rectangular ducts, *Int. J. Thermal Sci.*, **42**, pp. 187-198.
- [20] L. Wang and T. Yang, 2004, Bifurcation and stability of forced convection in curved ducts of square cross-section, *Int. J. Heat Mass Transfer*, **47**, pp. 2971-2987.
- [21] S. Yanase, R. N. Mondal, Y. Kaga and K. Yamamoto, 2005a, Transition from steady to chaotic states of isothermal and non-isothermal flows through a curved rectangular duct, *J. Phys. Soc. Japan*, **74** (1), pp. 345-358.
- [22] S. Yanase, R. N. Mondal and Y. Kaga, 2005b, Numerical study of non-isothermal flow with convective heat transfer in a curved rectangular duct, *Int. J. Thermal Sci.* (In Press).
- [23] R. N. Mondal, Y. Kaga, T. Hyakutake and S. Yanase, 2005, Unsteady solutions and the bifurcation diagram for the flow through a curved square duct, Submitted to *Fluid Dyn. Res.*